9th. International Conference on Concrete Block Paving. Buenos Aires, Argentina, 2009/10/18-21
Argentinean Concrete Block Association (AABH) - Argentinean Portland Cement Institute (ICPA)
Small Element Paving Technologists (SEPT)

OPTIMIZED NUMERICAL TOOL FOR THE ANALYSIS OF SEGMENTED CONCRETE BLOCK PAVEMENTS

OESER, Markus, markus.oeser@unsw.edu.au

CHANDRA, Herry, herwong15@yahoo.com

The University of New South Wales, School of Civil and Environmental Engineering (UNSW), Sydney, 2052, AUSTRALIA. Tel.: +61-2-93855016, Fax.: +61-2-93856139.

Note: The following is the notation used in this paper: (.) for decimals and ( ) for thousands.

Summary

A computational model for the analysis of segmented block pavements is presented in this paper. The model is based on the method of finite displacements elements. A three-dimensional Cosserat theory is applied to capture the displacements and the rotations of the single blocks within the finite elements. Constitutive relationships are introduced to account for the elastic and plastic behavior of the joint filling material. The model can be adjusted to a wide range of laying patterns and block shapes. The paper contains all relevant algorithms in matrix notation. The matrices are formulated in a way that a direct implementation into a displacement based three-dimensional finite element code is possible. The application of the model is presented by means of numerical simulations. The model is verified using large scale testing results.

1. INTRODUCTION

Segmented block pavements are often used as surface sealing for container yards, industry areas, aprons of airports, city roads etc. The extensive use of these pavements (especially in heavily loaded areas) requires efficient and accurate analysis and design methods. While substantial advances in the design of segmented block pavements have been made during recent years [Shackel, 2008], the analysis techniques used for these pavements still leave space for further improvement. The methods that are currently applied for this purpose are generally founded upon approximate techniques using the multilayer theory as analytical basis. The multi-layer theory is based on differential formulations of layered homogeneous continua. However, the prerequisites associated with the use of the multi layer theory are often in conflict with the discontinuous structure of segmented block pavements. Consequently, the results that are determined with the multi-layer theory may be different from the actual structural behavior of these pavements.

First attempts to overcome these deficiencies have been undertaken by [Oeser et al, 2007] where segmented block pavements are modeled using one or more finite elements for each block. This approach allows for a very detailed description of the interaction of the single blocks and can be used as a numerical tool to optimize block shapes and laying patterns in terms of their resistance against elastic and plastic deformations etc. In the model proposed by [Oeser et al, 2007] the blocks are treated as rigid bodies and only the joints can undergo deformations. Therefore it was possible to describe the displacements of the block surfaces by only 6 structural parameters per block (3 deformations and 3 rotations). The model was implemented into a software package and ready for application. Despite the relatively efficient way of modeling the displacements of the single blocks, the analysis of entire pavements remained unfeasible for the daily engineering practice due to too high computational time demand.

In contrast to the model proposed in [Oeser et al, 2007], the model presented in this paper captures the deformation behavior of entire domains of segmented block layers with finite displacement elements. Thereby, each finite element comprises a certain number of blocks. The displacements of the blocks (within the elements) are modeled by means of deformation shape functions as well as by an additionally introduced structural parameter, the so called Cosserat rotation. Interactions of the single blocks as well as inter-locking effects are accounted for using special interface-elements between the surfaces of adjacent blocks. Interactions between segmented block layers and underlying base and/or sub-base layers are taken into consideration by means of coupling elements. The deformation behavior of the joint filling material as well as the behavior of the base and sub-base materials is captured using elasto-plastic constitutive models.

2. SEGMENTED BLOCK LAYER

Figure 1 shows a layered pavement structure that consists of a surface layer formed by segmented concrete blocks, a bedding layer, an unbound granular layer and the subgrade. If required a frost protection layer may also be added between the unbound granular layer and the subgrade. The surface layer is modeled by two-dimensional discontinuous finite elements that are represented by the bold dotted lines in Figure 1. Each of these elements comprises a certain number of blocks. The elements are located in the middle plane of the surface layer. This plane is generally referred to as the reference plane.

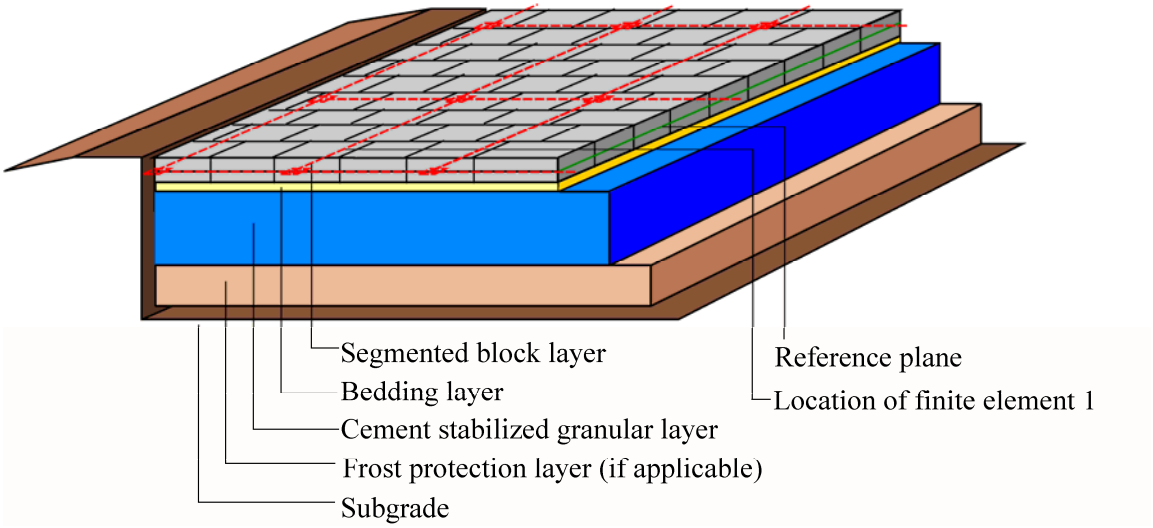


Figure 1: Segmented block pavement – FE mesh of the surface layer.

The left and the right side of Figure 2 present the discontinuous finite element used in the lower left corner of the pavement, see element 1 in Figure 1. This element comprises 12 blocks.

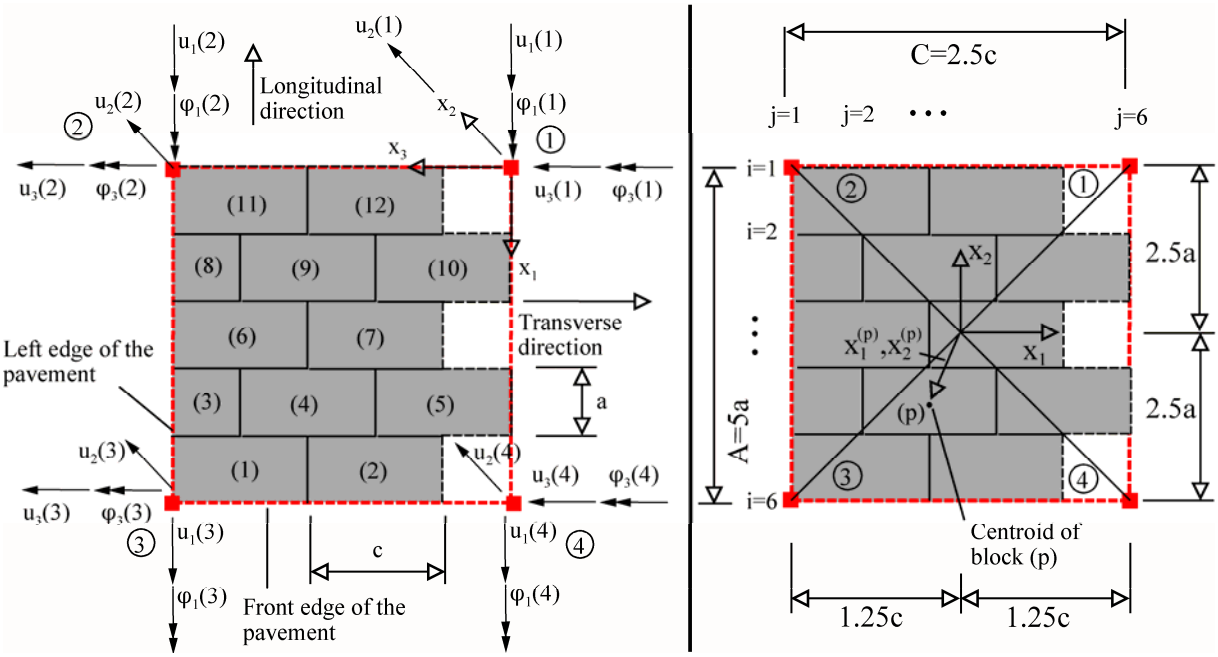


Figure 2: Two-dimensional discontinuous finite element.

2.1 Centroidal displacements of the blocks

Using the concept of finite elements it is assumed that (if the position of a block in an element is known) the displacements of the block can be calculated from the displacements and rotations of the element nodes. The displacements and rotations of the element nodes are denoted by $u_k(m)$ and φ_ℓ (m) with k=1,2,3, ℓ=1,3 and m=1,2,3,4, see Figure 2, left side. The calculation of the block displacements may be performed with equation (1).

$$u_k^{(p)} = u_k\left(x_1^{(p)}, x_2^{(p)}\right) = \sum_{m=1}^{n} N_m\left(x_1^{(p)}, x_2^{(p)}\right) \cdot u_k(m) = \sum_{m=1}^{n} N_m^{(p)} \cdot u_k(m) \qquad \textbf{(1)}$$

In equation (1) the variable $u_k^{(p)}$ represents the displacements of the centroid of block (p) in x_k-direction. $x_1^{(p)}$ and $x_2^{(p)}$ are the coordinates of the centroid of block (p) in the reference plane of the element. $N_m(x_1^{(p)}, x_2^{(p)}) = N_m^{(p)}$ are the shape functions of the element, see [Bathe, 2002]. The shape functions for the 4-node element displayed in Figure 2 are given in Equations (2a-d). The variable n in Equation (1) represents the number of nodes. Hence, n equals 4 if 4-node-elements are used for the analysis. Higher order elements, such as 8-node elements with 4 corner nodes and 4 edge nodes as well as 12-node elements with 4 corner and 8 edge nodes may also be used for the analysis. The advantage in using elements of higher order lies in a higher accuracy of the analysis results. However, using higher order elements yields higher computational effort and causes an increase in computational time need.

$$N_1(x_1, x_2) = \left(1 + 2 \cdot \frac{x_1}{C}\right) \cdot \left(1 + 2 \cdot \frac{x_2}{A}\right) \cdot \frac{1}{4} \qquad \textbf{(2a)}$$

$$N_2(x_1, x_2) = \left(1 - 2 \cdot \frac{x_1}{C}\right) \cdot \left(1 + 2 \cdot \frac{x_2}{A}\right) \cdot \frac{1}{4} \qquad \textbf{(2b)}$$

$$N_3(x_1,x_2)=\left(1-2\cdot\frac{x_1}{C}\right)\cdot\left(1-2\cdot\frac{x_2}{A}\right)\cdot\frac{1}{4} \qquad \textbf{(2c)}$$

$$N_4(x_1,x_2)=\left(1+2\cdot\frac{x_1}{C}\right)\cdot\left(1-2\cdot\frac{x_2}{A}\right)\cdot\frac{1}{4} \qquad \textbf{(2d)}$$

2.2 Centroidal rotations of the blocks

The rotations $\varphi_\ell^{(p)}$ of the centroids about the x_ℓ-axis (with ℓ=1,3) may be determined with Equation (3) wherein $\varphi_\ell(m)$ represents the rotations of the element nodes.

$$\varphi_\ell^{(p)}=\varphi_\ell\left(\xi_1^{(p)},\xi_2^{(p)}\right)=\sum_{m=1}^{n}N_m\left(\xi_1^{(p)},\xi_2^{(p)}\right)\cdot\varphi_\ell(m)=\sum_{m=1}^{n}N_m^{(p)}\cdot\varphi_\ell(m) \qquad \textbf{(3)}$$

The rotations $\varphi_2^{(p)}$ of the blocks about the x_2-axis must be determined from the first derivatives of the "in-plane" displacements $\partial u_1^{(p)}/\partial x_3$ and $\partial u_3^{(p)}/\partial x_1$. This is required to avoid relative displacements between adjacent blocks due to rigid body rotations of the element, see [Cerrolaza et al 1999].

$$\varphi_2^{(p)}=\frac{\partial u_1^{(p)}}{\partial x_3}-\frac{\partial u_3^{(p)}}{\partial x_1} \qquad \textbf{(4)}$$

However, research has shown, that Equation (4) restricts the movement of the blocks within an element to an extent where the results obtained with the computational model significantly deviate from the observations made in experiments, see [Cerrolaza et al 1999]. This problem may be overcome by introducing an additional structural parameter that is a rotation about the x_2-axis, see Figure 3. This additional parameter is called Cosserat-rotation. The "in-plane" rotation of the blocks is now determined with Equation (5).

$$\varphi_2^{(p)}=\varphi_2\left(\xi_1^{(p)},\xi_2^{(p)}\right)=\frac{\partial u_1^{(p)}}{\partial x_3}-\frac{\partial u_3^{(p)}}{\partial x_1}+\sum_{m=1}^{n}N_m^{(p)}\cdot\varphi_2(m) \qquad \textbf{(5)}$$

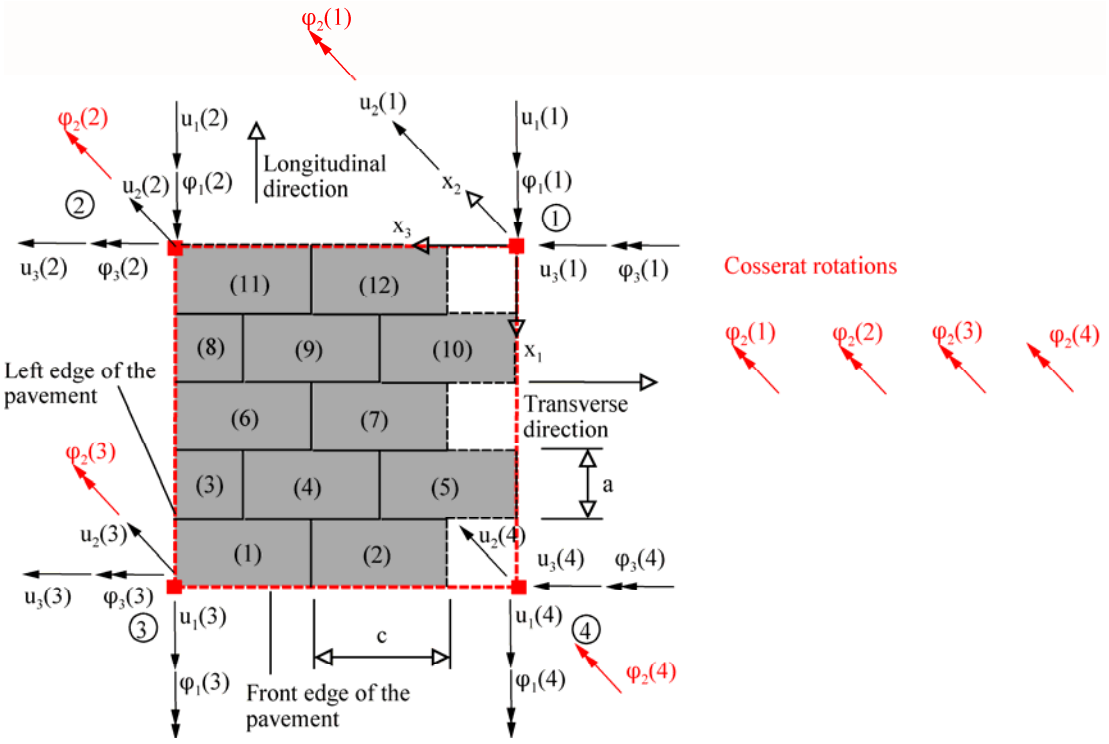


Figure 3: Two-dimensional discontinuous finite element with Cosserat rotations.

Equation (5) still fulfills the rigid body rotation criteria mentioned above and enhances the deformation approximation used in the finite element to better model the actual deformation behavior of segmented block layers.

2.3 Displacements of the block surfaces

Knowing the displacements and rotations of the centroids of the single blocks the displacements of the block surfaces can be determined. Therefore it is assumed that the blocks themselves do not change their geometry, i.e., the blocks behave like rigid bodies. This assumption implies that deformations in concrete block layers are only caused by changes in the geometry of the joints between the blocks and by block movements. The assumption seems reasonable as the stiffness of the concrete blocks exceeds the stiffness of the joint filling material by factor 100. Using this assumption the following relationship between the displacements of the block surfaces $u_1^{(p)}(q)$ and the displacements and rotations of the block centroids may be developed.

$$u_1^{(p)}(q) = u_1^{(p)} - x_2^{(p)}(q)\cdot\varphi_3^{(p)} + x_3^{(p)}(q)\cdot\varphi_2^{(p)} \qquad \textbf{(6a)}$$

$$u_2^{(p)}(q) = u_2^{(p)} + x_1^{(p)}(q)\cdot\varphi_3^{(p)} - x_3^{(p)}(q)\cdot\varphi_1^{(p)} \qquad \textbf{(6b)}$$

$$u_3^{(p)}(q) = u_3^{(p)} + x_2^{(p)}(q)\cdot\varphi_1^{(p)} - x_1^{(p)}(q)\cdot\varphi_2^{(p)} \qquad \textbf{(6c)}$$

In Equations (6a-c) $u_k^{(p)}(q)$ represents the displacements in x_k-direction of surface-point q, (with k=1,2,3 and q=1,2,…, 12), see Figure 4. The index p refers to the block number.

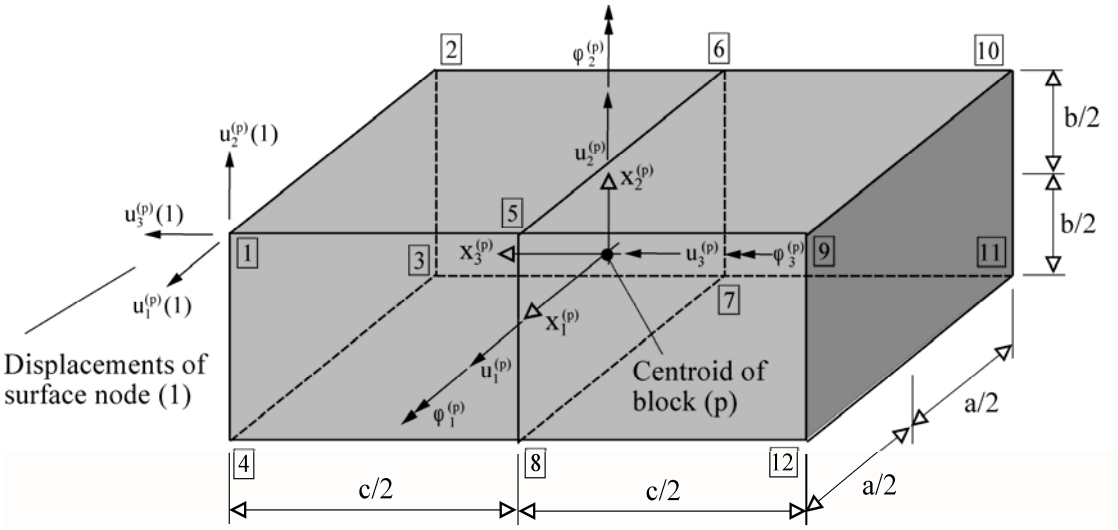


Figure 4: Rectangular block (p).

The spatial distances $x_k^{(p)}(q)$ measured from the bock centroid to the surface points (q) depend on the geometry of the block. For the simple rectangular block geometry chosen in Figure 4 the values of $x_k^{(p)}(q)$ are given by Equations 7a-c. For more complicated block geometries the values in Equation 7a-c must be adjusted. This may be done by defining a Cartesian coordinate system with its origin at the centroid of the block and measuring the distances from centroid to the surface points (q) along the axes of the system. The axes of the Cartesian system must be aligned in accordance to the coordinate system used for the determination of the displacements and rotations $u_k(m)$ and φ_ℓ (m) of the element nodes m.

$$x_1^{(p)}(q) = \pm a/2 \qquad \textbf{(7a)}$$

$$x_2^{(p)}(q) = \pm b/2 \qquad \textbf{(7b)}$$

$$x_3^{(p)}(q) = \pm c/2 \qquad \textbf{(7c)}$$

For the simple rectangular block geometry shown in Figure 4 the parameters a, b and c represent the length, width and height of the blocks.

2.4 Joint strains

The joints between the blocks are usually filled with sand of a certain grain size and grain size distribution. Occasionally, cement mortar is used as joint filling material (mostly in combination with cobblestones). Using cement mortar yields to an almost sealed surface through which hardly any water can infiltrate into the deeper layers. The use of cement mortar as joint material creates a very rigid surface and leads to ductile behavior of the block layer. This may yield to joint braking and loss of joint filling material. Concrete segmented block pavements with sand as joint filling material do not exhibit these problems. However, because of the lower stiffness and strength of the joint material higher elastic and plastic deformations of the joints may occur in these pavements. Elastic deformations of the joints can be accounted for in the computational model by very simple constitutive relationships such as Hooke's-law. To model plastic deformations of the joint filling material the plasticity concept according to Schofield and Worth may be used.

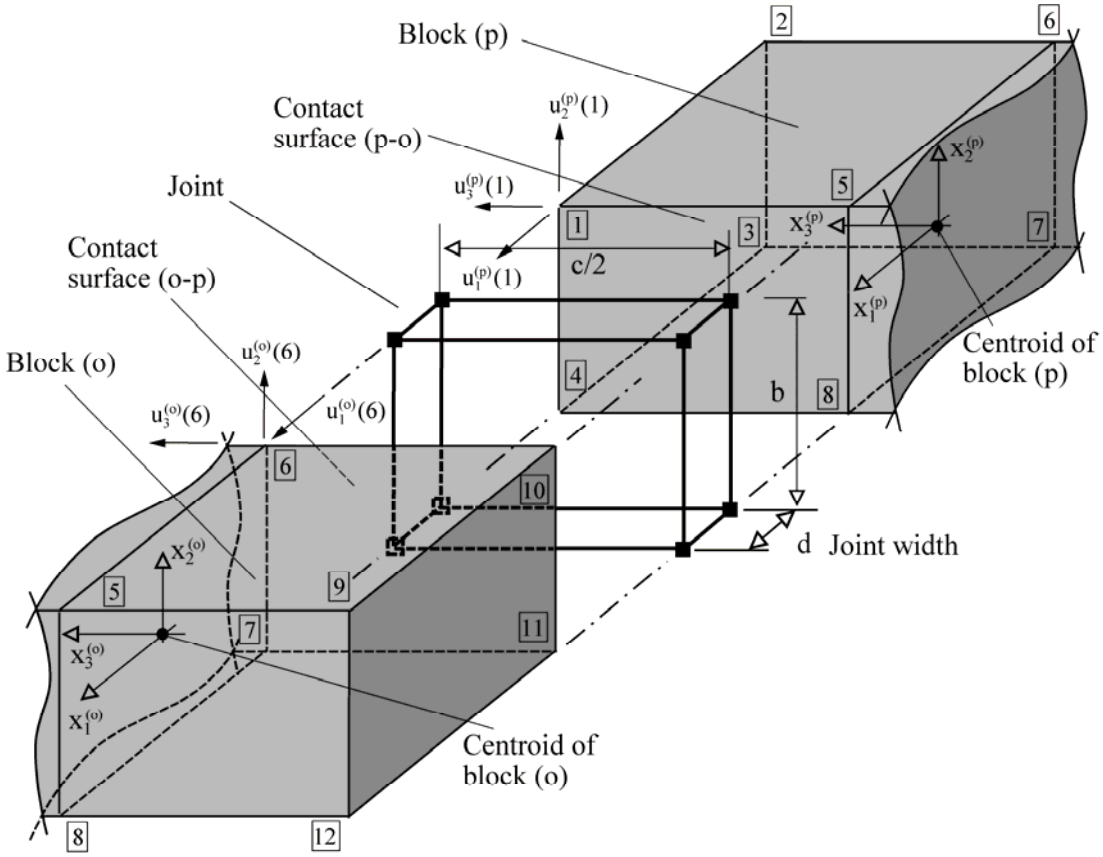


Figure 5: Blocks (p) and (o) including contact surfaces and joint.

To apply constitutive relationships the strains within the joints between the blocks must be known. The strain normal to the contact surface of adjacent blocks can be determined from the relative displacements of the block surfaces. As an example, Figure 5 shows two neighboring blocks (p) and (o) as well as the joint between them. The distance between the two blocks is drawn in an exaggerated manner in order to provide a better impression of the surface displacements and the block interaction. The determination of the normal strain $\varepsilon_1^{(o-p)}$ between these two blocks may be performed with Equation (8).

$$\varepsilon_1^{(o-p)} = \frac{\Delta u_1^{(o-p)}}{d} \qquad \textbf{(8)}$$

The variable $\Delta u_1^{(o-p)}$ in Equation (8) represents the relative displacements perpendicular to the contact surfaces (o-p) and (p-o) between opposite points of the contact surfaces. The joint width is denoted by parameter d in Equation (8). The strain $\gamma_2^{(o-p)}$ and $\gamma_3^{(o-p)}$ representing the distortion of the joint may be determined with Equations (9a-b).

$$\gamma_2^{(o-p)} = \frac{\Delta u_2^{(o-p)}}{d} \qquad \textbf{(9a)}$$

$$\gamma_3^{(o-p)} = \frac{\Delta u_3^{(o-p)}}{d} \qquad \textbf{(9b)}$$

The variable $\Delta u_2^{(o-p)}$ and $\Delta u_3^{(o-p)}$ in Equations (9a-b) represents the relative displacements parallel to the contact surfaces (o-p) and (p-o).

2.5 Joint stresses

It is assumed that the stresses in the joints are linked to the elastic components of the strain via Hooke's law. Hence, the normal joint stresses $\sigma_1^{(o\text{-}p)}$, $\sigma_2^{(o\text{-}p)}$ and $\sigma_3^{(o\text{-}p)}$ can be determined from the normal elastic joint strain ${}^{el}\varepsilon_1^{(o\text{-}p)}$.

$$\sigma_1^{(o-p)} = E^* \cdot (1-\nu) \cdot {}^{el}\varepsilon_1^{(o-p)} \qquad \textbf{(10a)}$$

$$\sigma_2^{(o-p)} = E^* \cdot \nu \cdot {}^{el}\varepsilon_1^{(o-p)} \qquad \textbf{(10b)}$$

$$\sigma_3^{(o-p)} = E^* \cdot \nu \cdot {}^{el}\varepsilon_1^{(o-p)} \qquad \textbf{(10c)}$$

The shear stresses $\tau_2^{(o\text{-}p)}$ and $\tau_3^{(o\text{-}p)}$ in the joints are to be determined from the elastic components of the joint distortion ${}^{el}\gamma_2^{(o\text{-}p)}$ and ${}^{el}\gamma_3^{(o\text{-}p)}$ using Equations (11a-b).

$$\tau_2^{(o-p)} = G^* \cdot {}^{el}\gamma_2^{(o-p)} \qquad \textbf{(11a)}$$

$$\tau_3^{(o-p)} = G^* \cdot {}^{el}\gamma_3^{(o-p)} \qquad \textbf{(11b)}$$

The parameters E* and G* must be determined with Equations (12a-b) wherein E represents the elasticity modulus and ν the Poisson's ratio of the joint material. These two parameters can be obtained from material tests.

$$E^* = \frac{E}{(1+\nu)\cdot(1-2\nu)} \qquad \textbf{(12a)}$$

$$G^* = \frac{E}{(1+\nu)} \qquad \textbf{(12b)}$$

As stated earlier, the plasticity concept according to Schofield and Worth is used to model the plastic joint strains ${}^{pl}\varepsilon_1^{(o\text{-}p)}$, ${}^{pl}\gamma_2^{(o\text{-}p)}$ and ${}^{pl}\gamma_3^{(o\text{-}p)}$. In order to use the plasticity concept the equivalent deviatoric stress $s_v^{(o\text{-}p)}$ and the mean normal stress $\sigma_m^{(o\text{-}p)}$ must be determined first.

$$\sigma_m^{(o-p)} = \frac{\sigma_1^{(o-p)} + \sigma_2^{(o-p)} + \sigma_3^{(o-p)}}{3} \qquad \textbf{(13)}$$

$$s_v^{(o-p)} = \sqrt{\frac{3}{2}\cdot\left(\left(\sigma_1^{(o-p)} - \sigma_m^{(o-p)}\right)^2 + \left(\sigma_2^{(o-p)} - \sigma_m^{(o-p)}\right)^2 + \left(\sigma_3^{(o-p)} - \sigma_m^{(o-p)}\right)^2 + \left(\tau_2^{(o-p)}\right)^2 + \left(\tau_3^{(o-p)}\right)^2\right)} \qquad \textbf{(14)}$$

Figure 6 contains a graphical representation of the yield concept according to Schofield and Worth. The curved solid line in Figure 6 is called yield surface and is generally denoted by Fy. Stress states inside the yield surface only cause elastic strain, while stress states at the yield surface trigger elastic and plastic strain. Stress states outside the yield surface can not exists as these stress states exceed the strength of the material. Stress states at the apex of the yield surface only yield distortion of the joint material. Plastic compression of the joint material is caused by stress states at the right side of the apex, and plastic dilatation is created by stress states at the left side of the apex. The right intersection point pb between the vertical axis and the yield function represents the strength of the joint material under three-dimensional compression. The left intersection point pa is to be interpreted as the strength of the material under three-dimensional tension. As unbound joint material does not possess any tensile strength the left intersection point coincides with the origin of the σm- sv-diagram.

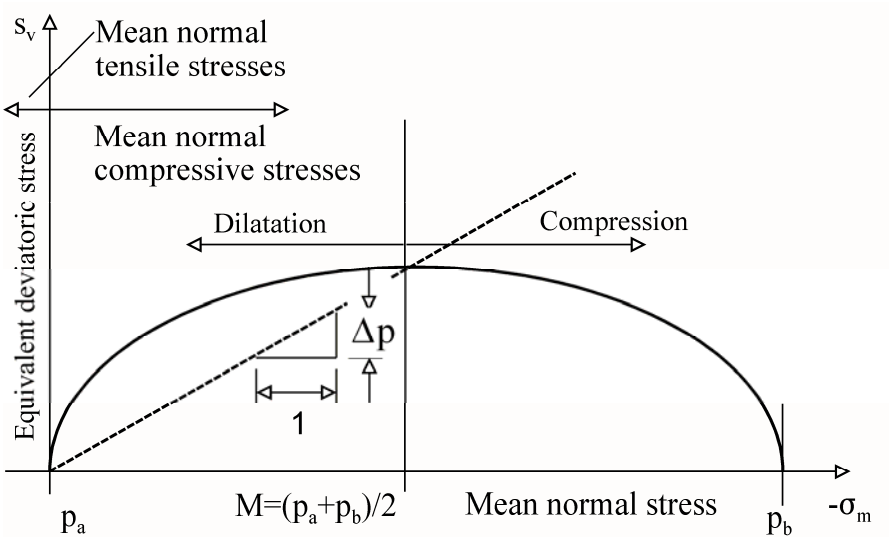


Figure 6: Yield surface according to Schofield and Worth.

The shape of the yield surface depends on the values p_a, p_b and Δp, which must be determined with material tests. Assuming associativity of the plastic flow the plastic strains may be determined from the yield surface F_y by means of Equation (15) and (16a-b).

$$ {}^{pl}\varepsilon_1^{(o-p)} = \lambda \cdot \frac{dF_y}{d\sigma_1} \qquad \textbf{(15)} $$

$$ {}^{pl}\gamma_2^{(o-p)} = \lambda \cdot \frac{dF_y}{d\tau_2} \qquad \textbf{(16a)} $$

$$ {}^{pl}\gamma_3^{(o-p)} = \lambda \cdot \frac{dF_y}{d\tau_3} \qquad \textbf{(16b)} $$

Because of the mathematical nature of the elasto-plastic constitutive relationships the determination of the stresses from the strain must be carried out iteratively. Firstly, it is assumed that the strains determined with the kinematic relationships (8) and (9a-b) are associated with a stress state that is inside the yield surface. This assumption implies that all strains are elastic. Secondly, the stresses are determined with Equations (10a-c) and (11a-b). Thirdly, the mean normal stress and the equivalent deviatoric stresses are determined and the assumption made above is verified. If the stress states is on the yield surface plastic strain are calculated using Equation (15) and (16a-b) and the elastic strain are determined with Equation (17) and (18a-b).

$$ {}^{el}\varepsilon_1^{(o-p)} = \varepsilon_1^{(o-p)} - {}^{pl}\varepsilon_1^{(o-p)} \qquad \textbf{(17)} $$

$$ {}^{el}\gamma_2^{(o-p)} = \gamma_2^{(o-p)} - {}^{pl}\gamma_2^{(o-p)} \qquad \textbf{(18a)} $$

$$ {}^{el}\gamma_3^{(o-p)} = \gamma_3^{(o-p)} - {}^{pl}\gamma_3^{(o-p)} \qquad \textbf{(18b)} $$

Fourthly, with the new elastic strain new stresses are determined. The process must be repeated until no further change in plastic strain occurs.

Stiffness of the Joints

The virtual work $\delta W^{(o\text{-}p)}$ of the joints is determined by multiplying the joint stresses with so called virtual joint strains $\delta\varepsilon_1^{(o\text{-}p)}$, $\delta\gamma_2^{(o\text{-}p)}$, $\delta\gamma_3^{(o\text{-}p)}$ and integration the product over the joint surface $A^{(o\text{-}p)}$.

$$\delta W^{(o-p)} = \int d \cdot \left(\delta\varepsilon_1^{(o-p)} \cdot \sigma_1^{(o-p)} + \delta\gamma_2^{(o-p)} \cdot \tau_2^{(o-p)} + \delta\gamma_3^{(o-p)} \cdot \tau_3^{(o-p)} \right) dA^{(o-p)} \qquad \textbf{(19)}$$

The joint strains and joint stresses can be related to the displacements and rotations of the element nodes (see Figure 3) via the constitutive and kinematic relationships derived above. Therefore it is possible to express Equation (19) in dependency of the displacements and rotations of the nodes rather than in dependency of the joint strains and stresses. Furthermore it is possible to isolate the nodal displacement and rotations from the integral in Equation (19) so that Equation (20) can be formulated.

$$\delta W^{(o-p)} = \delta \underline{u}^T \cdot \underline{K}^{(o-p)} \cdot \underline{u} \quad \text{with} \quad \underline{u}^T = \begin{bmatrix} u_1(1) & u_1(1) & \cdots & \varphi_3(4) \end{bmatrix} \quad \text{and} \quad \underline{u} = \begin{bmatrix} u_1(1) \\ u_2(1) \\ \vdots \\ \varphi_3(4) \end{bmatrix} \qquad \textbf{(20)}$$

The steps that must be carried out to transform Equation (19) to Equation (20) are not discussed in the paper as they are based on standard techniques that are commonly used in finite element developments. Readers desiring more information on these techniques may be referred to [Bathe 2002]. The vector $\underline{u}$ in Equation (20) contains the displacements and rotations of the element nodes in vector notation. $\underline{K}^{(o\text{-}p)}$ is the joint matrix representing the stiffness of joint (o-p) against the displacements and rotations of the nodes of the element. To account for all joints within the element the single joint matrices must be added up to the element stiffness matrix $\underline{K}$.

$$\underline{K} = \sum_s \underline{K}^{(o(s)-p(s))} \qquad \textbf{(21)}$$

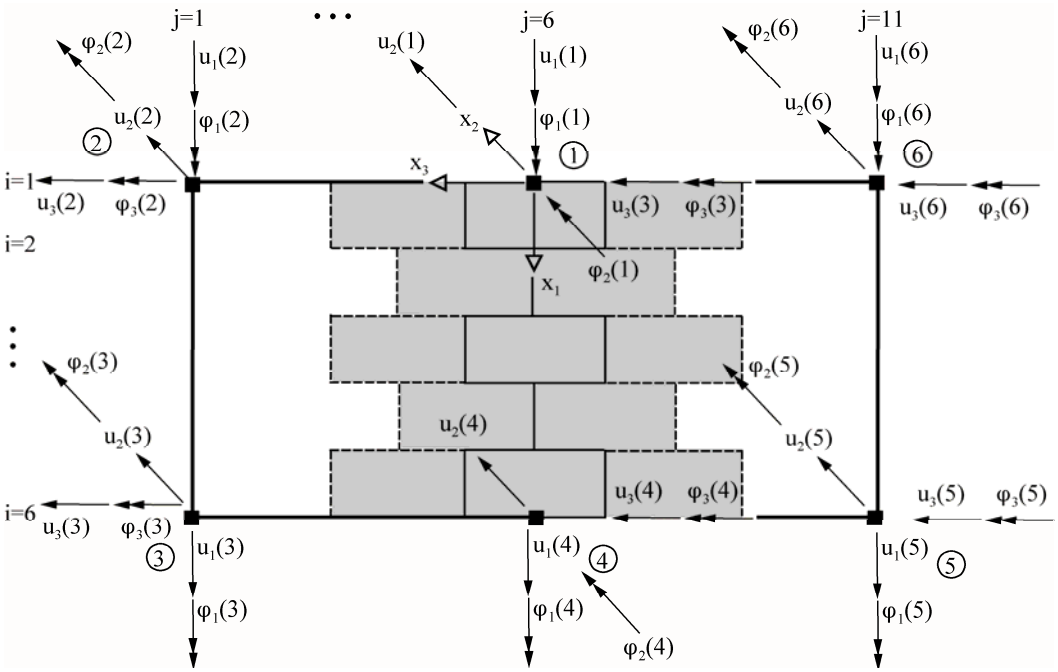


Figure 7: Discontinuous finite element.

In Equation (21) the variable s represents the total number of joint in an element. The element shown in Figure 3 comprises 23 joints (solid lines between the blocks). The dotted joint lines in Figure 3 represent joints with blocks that are partly or entirely in the domain of adjacent finite elements. To capture the stiffness of these joints a second discontinuous finite element is used, see Figure 7. This element comprises 16 joints.

3. BASE AND SUBBASE LAYERS

The base and subbase layers are modeled with three-dimensional finite elements with 8 nodes. The nodes are located in the element corners. Alternatively 20 node elements with 8 corner nodes and 12 edge nodes or 32 node elements with 8 corner nodes and 24 edge nodes can be used. The number and positions of the element nodes as well as the geometry of the elements must be aligned to the element mesh used to model the segmented block layer. In other words, the elements used for the different layers must be placed on to of each other, see Figure 8. In order to avoid displacement discontinuities between the element edges all nodes at the contact surfaces between neighboring elements must be coupled. Hence, if 4 node 2d-elements shall be used to model the displacement behavior of the segmented block layer, 8 node 3d-elements must be used for the base and subbase layers. The use of 8 node 2d-elements for the segmented block layer requires 20 node 3d-elements for the base and sub-base layers etc.

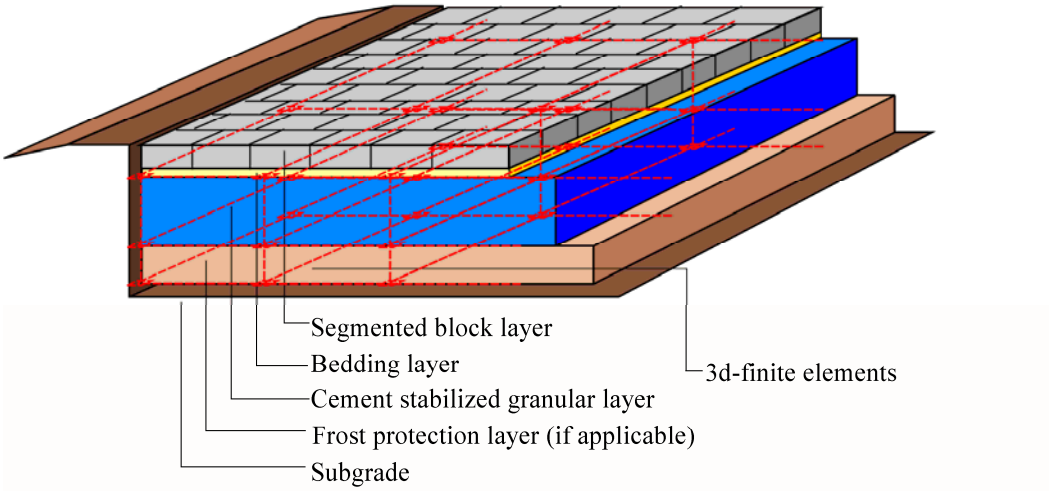


Figure 8: Segmented block pavement – FE mesh of the base and sub-base layers.

Unbound granular materials are frequently used for base and sub-base layers. This type of material can also be modeled by the constitutive relationships discussed in section 2.5. In this case the complete three-dimensional stress strain state (σ_k, τ_k, ε_k, γ_k with k=1,2,3) must be taken into account. This may be achieved by an extension of Equations (10a-c), (11a-b), (13), (14), (15) and (16a-b).

3.1 Elastic constitutive relationships

$$\sigma_k = E^* \cdot \left((1-\nu) \cdot {}^{el}\varepsilon_k + \sum_{\ell \neq k} \nu \cdot {}^{el}\varepsilon_\ell \right) \quad \text{with } k = 1,2,3 \text{ and with } \ell = 1,2,3 \qquad \textbf{(22)}$$

$$\tau_k = \frac{G^*}{2} \cdot {}^{el}\gamma_k \quad \text{with } k = 1,2,3 \qquad \textbf{(23)}$$

3.2 Plastic constitutive relationships

$$s_v = \sqrt{\frac{3}{2} \cdot \left(\left(\sigma_1 - \sigma_m\right)^2 + \left(\sigma_2 - \sigma_m\right)^2 + \left(\sigma_3 - \sigma_m\right)^2 + \left(\tau_1\right)^2 + \left(\tau_2\right)^2 + \left(\tau_3\right)^2 \right)} \qquad \textbf{(24)}$$

$$^{pl}\varepsilon_k = \lambda \cdot \frac{dF_y}{d\sigma_k} \text{ with } k = 1,2,3 \qquad \textbf{(25)}$$

$$^{pl}\gamma_k = \lambda \cdot \frac{dF_y}{d\tau_k} \text{ with } k = 1,2,3 \qquad \textbf{(26)}$$

4. BEDDING LAYER

The modeling of the bedding layer can be conducted similarly to the modeling of the joints. In this case the relative displacements within the bedding layer are determined from the displacements of the lower surface of the blocks and the displacements of the upper surface of the base layer, see Figure 9. To model the elastic and plastic behavior of the bedding material the same constitutive relationships may be used as for the joint filling material.

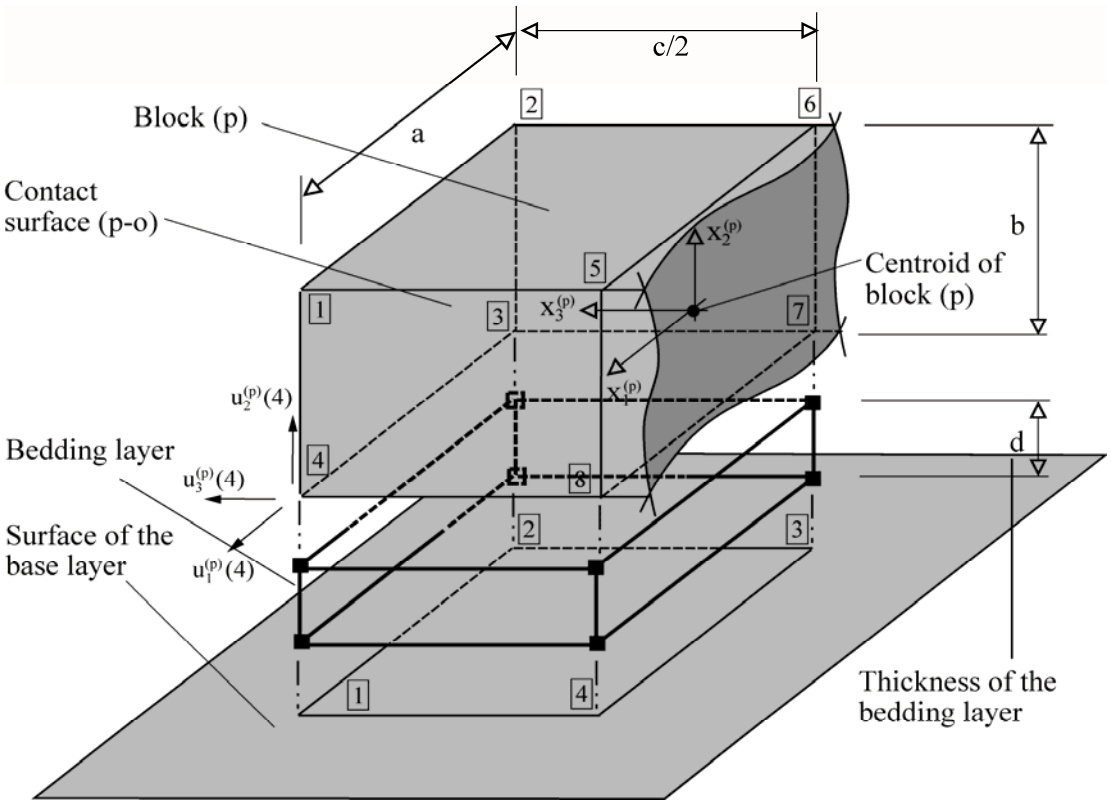


Figure 9: Blocks (p), bedding layer and surface of the base layer.

5. SUBGRADE

An efficient way of modeling the subgrade is given by the boundary element method, see (Moeller et al 2004). Using the boundary element method it is only necessary to mesh the surface of the subgrade. This significantly reduces the computational effort compared with the modeling based on the finite element method, where a three-dimensional domain of the subgrade must be meshed. The

use of the boundary method implies that the subgrade is treated as semi-infinitely extended homogeneous continuum with linear elastic material behavior.

6. NUMERICAL SIMULATIONS

In (Oeser et al, 2007) the deformation behavior of segmented block pavements was studied on the basis of large scale laboratory tests and numerical simulations. As mentioned above it was possible to accurately model the behavior of the pavements and to predict the elastic and plastic deformations observed in the laboratory. However, the model used in (Oeser, et al 2007) would capture the displacements and rotations of each block by 6 structural parameters, which led to very accurate results but also to high computational time needs. Scope of this section is to demonstrate that the model proposed in section 2 to 4 is capable of significantly reducing the computational effort without losing the accuracy achieved with the model in (Oeser et al 2007).

The segmented block pavement investigated in this study consists of 15 x 30 blocks. The length of the blocks is 200mm and their width is 100mm. The blocks are 80mm thick. The laying pattern is equal to the pattern shown in Figure 3. The total area of the pavement considered in this study was 1500mm x 3000mm. The loaded area was 300mm x 300mm. More detailed material and geometry data are given in (Ascher et al 2007). The FE-mesh used for the segmented block layer comprised 6 by 6 elements. For the base layer and the subgrade the same raster was used. In vertical direction the base layer was modeled by 5 elements.

The solid line in Figure 10 represents the accumulated horizontal deformation of the blocks after 10.000 load cycles along the load axis obtained with the model used in (Oeser et al 2007). The computational time was 45 seconds per load cycle using a 1.86 GHz Intel Processor. Line 1 in Figure 10 represents the results using the model proposed in section 2 to 4 in combination with the 4 node 2d-elements for the block layer and the 8-node elements for the base layer. The computational time was only 0.4 seconds. Line 2 shows the results obtained with 8 node 2d-elements and 20-node 3d-elements. 12 node 2d-elements and 32 node 3d-elements have been used to produce the results represented by curve 3. The computational time to produce the results of line 2 was 3.9 seconds per cycle. 10.9 seconds per cycle were needed to create the results curve 3 is based on.

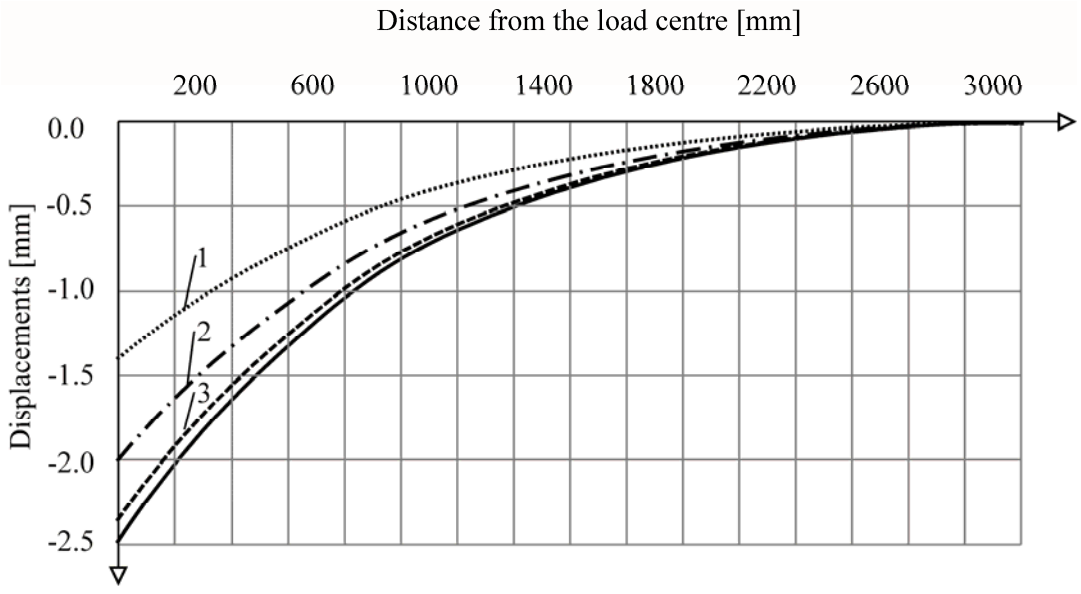


Figure 10: Results of numerical simulations.

7. CONCLUSION

The results presented in Figure 10 indicate that the model discussed in section 2 to 4 can reproduce the results obtained in previous research (solid line in Figure 10). The accuracy of the results is strongly dependant on the order of the shape function of the finite elements (e.g. 4 node, 8 node or 12 node 2d-elements and 8 node, 20 node and 32 node 3d-elements) and also on the density of the mesh. If 12 node 2d-elements and 32 node 3d-elements are used, the model is capable of reproducing the results of the previous research reasonably well. In this case, the model accelerates the computational process by the factor of 4 (45 seconds over 10.9 seconds). If elements with less nodes are used the computational time need reduces even more. However, the reduction in computational time is achieved at the expenses of accuracy of the results, (see curve 1 and 2 in Figure 10).

It must be noted that even with the newly developed model the analysis of 10.000 load cycles still takes approximately 30h. Further developments and ongoing improvements in computational techniques will be necessary to reduce the computational time to an extent, where the newly developed methods may be adopted for the daily engineering design processes.

8. REFERENCES

SHACKEL, B., 2008. Design of Permeable Pavements for Australian Conditions. Proceedings of the 23rd ARRB Conference – Research Partnering with Practitioners, Adelaide, Australia.

OESER, M., ASCHER, D., LERCH, T., WELLNER, F., 2007. Load-bearing Behavior of Pavement Structures – Development of a Numerical Design Program, International Journal of Concrete Plant + Precast Technology (BFT), Vol. 73, pp. 4-13.

BATHE, K.-J., 2002. Finite-Elemente-Methoden, Springer Verl., Berlin, 2002.

CERROLAZA, M. SULEM, J. ELBIED, A., 1999. A Cosserat non-linear Finite Element Analysis Software for Blocky Structures, Advances in Engineering Software 30, pp. 69–83.

MÖLLER, B., OESER, M., 2002. FE-BE Computational Model for Multi-Layered Road Constructions.

In: Scarpas, A.; Shoukry, S. N. (ed.), Third International Symposium – 3D Finite Element Modeling of Pavement Structures, Amsterdam, pp. 209-234.

ASCHER, D., LERCH, T., WELLNER, F., 2007. Deformation behavior of concrete block pavements under vertical and horizontal dynamic load, International Journal of Concrete Plant + Precast Technology (BFT), Vol. 73, pp 16-23.